

# Edge Contamination Effects in the Dynamics of Vortex Matter in Superconductors: Memory Effects and Excess Flux-flow Noise

G. Jung<sup>1,2</sup>, Y. Paltiel<sup>2,3</sup>, E. Zeldov<sup>2</sup>, Y. Myasoedov<sup>2</sup>, M.L. Rappaport<sup>2</sup>, M.J. Higgins<sup>4</sup>, and S. Bhattacharya<sup>4,5</sup>

<sup>1</sup> Ben Gurion University of the Negev, Department of Physics, Beer-Sheva 84105, Israel

<sup>2</sup> Weizmann Institute of Science, Department of Condensed Matter Physics, Rehovot 76100, Israel

<sup>3</sup> Electro-Optics Division, Soreq NRC, Yavne 81800, Israel

<sup>4</sup> NEC Research Institute, Princeton, New Jersey 08540, USA

<sup>5</sup> Tata Institute of Fundamental Research, Mumbai-400005, India

The magnetic flux line lattice in type II superconductors serves as a useful system in which to study condensed matter flow, as its dynamic properties are tunable. Recent studies have shown a number of puzzling phenomena associated with vortex motion, including: low-frequency noise and slow voltage oscillations; a history-dependent dynamic response, and memory of the direction, amplitude duration and frequency of the previously applied current; high vortex mobility for alternating current, but no apparent vortex motion for direct currents; negative resistance and strong suppression of an a.c. response by small d.c. bias. A generic edge contamination mechanism that comprehensively accounts for these observations is based on a competition between the injection of a disordered vortex phase at the sample edges, and the dynamic annealing of this metastable disorder by the transport current. For an alternating current, only narrow regions near the edges are in the disordered phase, while for d.c. bias, most of the sample is in the disordered phase-preventing vortex motion because of more efficient pinning. The resulting spatial dependence of the disordered vortex system serves as an active memory of the previous history. Random injection of the strongly pinned metastable disordered vortex phase through the sample edges and its subsequent random annealing into the weakly pinned ordered phase in the bulk results in large critical current fluctuations causing strong vortex velocity fluctuations. The resulting excess low frequency flux-flow voltage noise displays pronounced reentrant behavior. In the Corbino geometry the injection of the metastable phase is prevented and, accordingly, the excess noise is absent.

## 1 Introduction: Vortex Matter

Type-I superconductors undergo a first-order transition from the superconducting state, with total magnetic flux expulsion (Meissner effect), to the normal state at a critical field  $H_c$ . In marked contrast, type-II superconductors above a lower critical field  $H_{c1}$  allow magnetic flux to penetrate in a regular array of quantum units of  $\Phi_0 = h/2e$ , each flux tube being confined by a circulating vortex of current. These materials remain superconducting until a second-order transition at an upper critical field  $H_{c2}$ . The magnetic flux vortices in type-II superconductors were predicted by A. Abrikosov in 1957 in his ground-breaking paper based on the Ginzburg-Landau theory. The achievements of V. Ginzburg and A. Abrikosov were honored by the Nobel committee only last year, some 30 years after granting the prize for the BCS theory, published in the same year as the Abrikosov paper, and almost two decades after awarding the Nobel prize for the 1986 break-through discovery of new classes of oxide-based high-temperature superconductors. This discovery extended the range of the phase diagram, within which the superconducting vortices exist, by orders of magnitude, making investigation of the vortex matter one of the most vigorous research areas in solid state physics [1–4].

When transport current flows through a superconducting specimen in a mixed state, i.e., the state containing magnetic flux vortices, a Lorentz force acts on the flux tubes causing them to move in a direction perpendicular to the current flow. Unless vortex motion is prevented by pinning (jamming) of the vortices on intrinsic and artificially introduced material imperfections, voltage appears across the specimen and energy is dissipated. However, even in the presence of pinning centers, the vortex system yields and starts to move at currents higher than the so-called critical depinning current.

The onset of motion is accompanied by significant low frequency noise. The fluctuations peak in close vicinity to the “peak effect”, where the critical current anomalously increases with increasing temperature. Excess low frequency noise at the peak effect is accompanied by a series of exotic and puzzling phenomena associated with vortex motion, such as slow voltage oscillations, history-dependent dynamic response, and memory of the direction, amplitude, duration and frequency of the previously applied current, high vortex mobility for alternating current, but no apparent vortex motion for direct currents, and strong suppression of an a.c. response by a small d.c. bias. Taken together, these phenomena can be comprehensively explained by a model that accounts for contamination of the ordered vortex phase by a disordered vortex phase created by vortices penetrating irregular sample edges [5]. In this paper we concentrate on how edges influence dynamic instabilities, memory, and noise in the vortex system.

## 2 Edge Contamination

Our current understanding of the peak effect (PE) is that it is due to a first order phase transition between a quasi-ordered weakly pinned Bragg glass-like vortex phase below the PE and a strongly pinned disordered phase (DP) of solid vortex matter within and above the PE. The order-disorder phase transition of the vortex lattice occurring between the two solid vortex matter phases allows for the existence of a supercooled metastable DP in the part of the phase diagram occupied by the equilibrium ordered phase (OP). At temperatures well below the PE the supercooled phase is very fragile and any small perturbation, such as transport current, will easily anneal it into the equilibrium OP. However, at temperatures only slightly below the PE the applied current will have two competing effects: on the one hand it will anneal the disorder, but on the other hand, it will contaminate the system by fresh penetration of DP resulting in dynamic coexistence of the two phases. The injection of the disordered vortex phase through the sample edges is the core of the edge contamination (EC) mechanism.

Current flow in a superconducting sample containing the equilibrium ordered vortex phase well below the phase transition results in uniform motion of the entire vortex lattice. The penetrating vortices enter at their proper lattice locations and the order of the lattice is preserved. The presence of surface barriers in real samples significantly changes the situation. The barrier height is sensitive to the surface quality; vortices penetrate predominantly at the weakest spots of the barrier, and locally destroy the ordered lattice. Far below the phase transition the disordered state is highly unfavorable energetically and anneals rapidly into OP. However, in the close vicinity below the order-disorder phase transition a metastable DP will be formed near the sample edge. Since the free energies of the two phases are comparable near the phase transition, the metastable DP becomes sufficiently stable on the relevant experimental time scales to gradually penetrate deep into the sample with the flow of the entire lattice [5–7]. The DP can be pinned more efficiently and is characterized by significantly larger critical current than the weakly pinned ordered vortex phase [8–11]. The contamination process thus causes an enhancement of the total integrated critical current of the sample. A strongly pinned metastable disordered vortex phase dynamically anneals in the bulk into an ordered phase with much smaller critical current. The applied current, therefore, has two effects: the current that flows at the edges causes “contamination” by injecting a disordered vortex phase, while the current that flows in the bulk acts as an annealing mechanism. The ensemble of puzzling phenomena observed in the vicinity of the peak effect and discussed in detail below arises because of the dynamic balance between these two competing processes.

## 2.1 Critical Current in the Edge Contamination Model

Let us characterize the DP by the local critical current density  $J_c(x)$  at a distance  $x$  from the edge, which has a non-equilibrium excess value  $\tilde{J}_c(x) = J_c(x) - J_c^{ord}$  relative to the critical current of the fully ordered phase. Since in low-temperature superconductors thermal activation is negligible, the sole annealing mechanism is current-driven displacement that promotes rearrangement of the vortices during their motion. The relative change of  $\tilde{J}_c$  upon displacement by a small  $\Delta x$  is therefore given by  $\Delta x/L_r$ , where  $L_r$  is a characteristic relaxation length over which the DP anneals into the OP. Since the lattice flows with velocity  $v$ ,  $\tilde{J}_c$  at  $x + \Delta x$  and at time  $t + \Delta t = t + \Delta x/v$  is thus described by  $\tilde{J}_c(x + \Delta x, t + \Delta x/v) = \tilde{J}_c(x, t)(1 - \Delta x/L_r)$ , which leads to the partial differential equation for the annealing process [14]

$$\partial \tilde{J}_c(x, t) / \partial x + (1/v) \partial \tilde{J}_c(x, t) / \partial t = -\tilde{J}_c(x, t) / L_r(v), \quad (1)$$

The boundary condition at  $x = 0$ , where vortices penetrate into the sample, is  $\tilde{J}_c(0, t) = J_c^{dis} - J_c^{ord}$ , where  $J_c^{dis}$  is the critical current of the totally disordered phase. A key aspect of the annealing process is that the relaxation length  $L_r$  crucially depends on the displacement velocity  $v$  and on the proximity to the phase transition. Close to the phase transition the metastable DP is rather stable and  $L_r$  is large. Deeper into the OP region the metastable phase becomes more and more unstable,  $L_r$  is small and  $J_c$  is depressed. Theoretical considerations [15, 16] and fast transient measurements [9] show that  $L_r$  decreases with increasing vortex displacement velocity according to an empirical relation  $L_r \simeq L_0(v_0/v)^\eta = L_0(V_0/V)^\eta$ . Here  $\eta$  is typically in the range of 1 to 3,  $L_0$ ,  $v_0$ , and  $V_0$  are scaling parameters,  $V = vBl$  is the measured voltage drop,  $B$  is the magnetic field, and  $l$  is the distance between the voltage contacts.

The d.c. solution of (1) is  $J_c^{dc}(x) = (J_c^{dis} - J_c^{ord}) \exp(-x/L_r) + J_c^{ord}$  and the integrated d.c. critical current becomes:

$$I_c = d \int_0^W J_c^{dc}(x) dx = (J_c^{dis} - J_c^{ord}) [1 - e^{-\frac{W}{L_r(V)}}] L_r(V) d + I_c^{ord}, \quad (2)$$

where  $I_c^{ord} = J_c^{ord} W d$ ,  $W$  is the sample width and  $d$  its thickness. Observe, that  $I_c$  depends on  $L_r$ , which in turn depends on the voltage  $V$ .

To evaluate the shape of the  $V - I$  characteristics in the edge contamination model assume, for simplicity, that the flux-flow resistance  $R_f$  is the same for the DP and the OP and that the asymptotic  $V - I$  characteristics for the DP and OP are  $V = R_f(I - I_c^{dis})$  and  $V = R_f(I - I_c^{ord})$ , respectively. When the DP and OP coexist,  $V = R_f(I - I_c)$  with the voltage dependent  $I_c$  given by 2. An example of the non-linear  $V - I$  characteristic obtained by means of numerical simulations is shown in Fig. 1. At very low voltages,  $L_r$  is larger than the sample width, the entire sample is contaminated by the DP, and the  $V - I$  curve initially follows the asymptotic dashed line of the DP

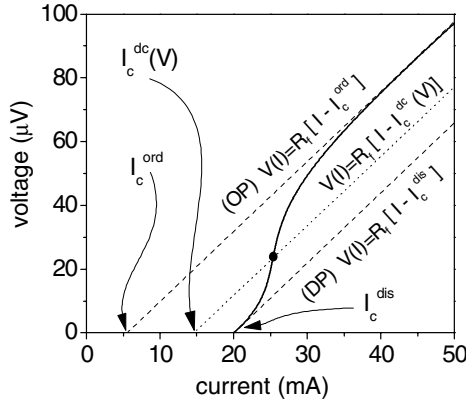


**Fig. 1.** Calculated  $V-I$  characteristic (*solid line*) of coexisting vortex phases based on (2). The asymptotic characteristics of fully ordered and fully disordered vortex phases are shown with *dashed lines*

with  $I_c = I_c^{dis}$ , where  $I_c^{dis} = J_c^{dis} W d$ . At high vortex velocities,  $L_r$  becomes very short, most of the sample is in the OP, and the  $V-I$  approaches the asymptotic line of the OP with  $I_c = I_c^{ord}$ . In the crossover region, due to a continuous decrease with current of the total  $I_c$ , a nonlinear  $V-I$  characteristic is obtained. The curvature in the crossover region depends on the parameters  $\eta$ ,  $L_0$ , and  $V_0$ . Our numerical simulations show that with rapidly decreasing  $L_r$  one may even obtain a negative slope resulting in S-shaped  $V-I$  characteristics.

## 2.2 Strip and Corbino Configuration

In the Corbino disk geometry, the vortices circulate in the bulk without crossing the sample edges. In such an arrangement the contamination by DP is avoided and the true bulk properties of the vortex matter can be investigated [6,12,13]. In order to perform transport and noise measurements in both the Corbino and strip-like geometry on the same crystal we have prepared a special contact configuration, seen in the inset in Fig. 2b [6]. All experiments discussed in this paper were performed on Fe-doped (200 ppm) 2H-NbSe<sub>2</sub> single crystals with  $T_c = 5.6$  K, which display a significantly broader PE as compared to pure crystals. However, additional experiments performed using samples with different doping showed the same general behavior as the one described here. This leads us to believe that the observed phenomena are common to all superconductors exhibiting PE and are not sample dependent.

Figure 2a shows the d.c. voltage response  $V$  vs. the magnetic field applied parallel to the crystal  $c$ -axis at 4.4 K in the strip and Corbino disk configuration. Since in the Corbino disk the current density varies across the sample, we have applied different driving currents in the two geometries in

order to have the same average current density between  $+V$ ,  $-V$  contacts in both arrangements. As a result, the measured  $V$  and the corresponding vortex velocity are identical at high fields. Upon decreasing the field from above  $H_{c2}(T)$ , the voltage decreases rapidly and vanishes in the PE region (4 to 8 kOe), where  $I_c$  of the sample is large due to the presence of the strongly pinned DP. The voltage appears again at intermediate fields between the phase transition fields  $H_{DT}$ . In this field range the voltage in the Corbino disk increases linearly with  $H$ , consistent with the well-known flux-flow behavior, indicating that the flowing lattice is in the ordered phase. The sharp drop of the voltage response at each  $H_{DT}$  is due to an abrupt disorder-driven transition of the equilibrium OP into a highly pinned equilibrium DP. The existence of two transition fields indicates the reentrant behavior of the equilibrium DP in Fe doped NbSe<sub>2</sub> [6, 17, 18]. The region of phase coexistence, seen in Fig. 2b, appears always on the Bragg glass side of the transition. Therefore at low fields we face a mirror-like image of high field behavior, see Fig. 2b.

The voltage response of the strip configuration is restricted to a narrower field range contained between high and low onset fields  $H_{on}^s$ . The strip voltage is strongly suppressed relative to the Corbino, indicating stronger effective pinning as a result of an intermixture of DP with OP due to the

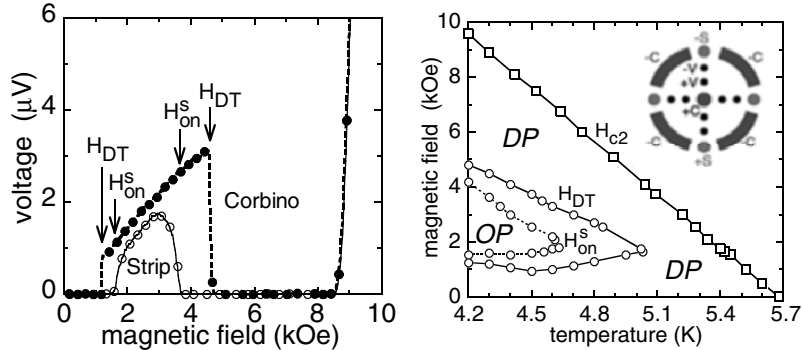


**Fig. 2.** (a) d.c. voltage seen in a Fe-doped NbSe<sub>2</sub> sample in Corbino and strip geometries. The currents in both geometries were adjusted to provide equal current densities in the vicinity of the voltage contacts. (b) Phase diagram of vortex matter in the same sample as in a). Dynamic coexistence of DP and OP occurs in the area contained between the  $H_{DT}$  and  $H_{on}^s$  lines. Inset: contact configuration enabling measurements in both Corbino and strip geometry. By applying the current to the  $+S$ ,  $-S$  contacts, the vortices penetrate through the edge and flow across the sample, similarly to the standard strip configuration. In contrast, by applying the current to the  $+C$ ,  $-C$  contacts, the vortices circulate in the bulk without crossing the edges, as in a Corbino disk. In both configurations the voltage and the corresponding noise are measured across the same contacts  $+V$ ,  $-V$ . The distance between the voltage contacts is 0.15 mm and the Corbino disk diameter is 1.1 mm

EC mechanism. Figure 2b shows the phase diagram of the iron-doped NbSe<sub>2</sub> determined by transport measurements of the Corbino and strip geometries.

### 3 Memory Effects, Dynamical Instabilities and Edge Contamination

Many experiments performed in the past decade have demonstrated several surprising phenomena in the low frequency response of the vortex matter in conventional [8, 9, 19–22, 24, 25] and high- $T_c$  superconductors [27–33]. These phenomena were particularly pronounced in 2H-NbSe<sub>2</sub> strips in the vicinity of the peak effect, where an ordered vortex lattice transforms into a highly disordered one. Among the most striking phenomena are the memory effects, in which the vortex system remembers the direction, amplitude, duration, and even the frequency of the previously applied current [24–26], and the history dependent dynamic response [8, 9, 21–23]. High vortex mobility is observed in the presence of a.c. transport current while the vortices appear to be immobile in the presence of d.c. current of the same or even substantially larger amplitude [24]. Moreover, the addition of a small d.c. current to a large a.c. current can fully suppress the a.c. response of the system [24]. Figure 3 shows a.c. resistance  $R_{ac}$  of a 2H-NbSe<sub>2</sub> sample recorded as a function of a superposed d.c. current  $I_{dc}$ . Note that the addition of only 10 to 20% of  $I_{dc}$  suppresses the a.c. response  $R_{ac}$  by orders of magnitude.

The edge contamination model can account for all the strange phenomena associated with the peak effect in terms of the competition between injection of a disordered vortex phase through the surface barriers at the sample edges, and annealing of the metastable disorder by the transport current [5]. The key

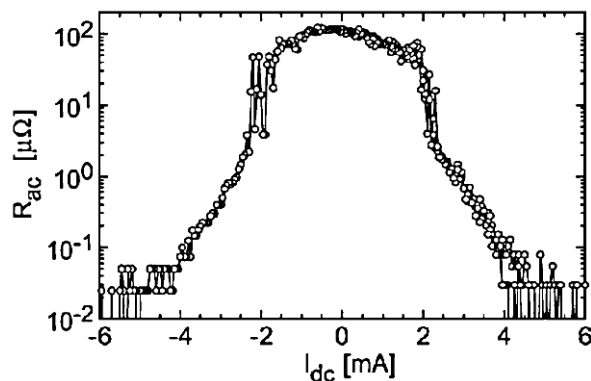


**Fig. 3.** a.c. resistance  $R_{ac}$  of a 2H-NbSe<sub>2</sub> as a function of the superposed d.c. bias in the vicinity of the peak effect. The experimental data were obtained for a.c. bias current  $I_{ac} = 20$  mA, frequency  $f = 181$  Hz,  $B = 400$  mT, and  $T = 5$  K

element of the edge contamination model is the spatial variation of the structural disorder in the vortex matter resulting in position dependent  $J_c(x)$ , as outlined in the Sect. 2.1. Correspondingly, transport current becomes nonuniform and follows the distribution  $J_c(x)$ . The EC model predicts that when a strip is biased with a d.c. current a significant part of the sample will be filled with the disordered phase injected through an edge. Strong pinning of the DP prevents vortex motion and one should expect a low response. If the d.c. bias is substituted by an a.c. current then only narrow regions near the edges will be contaminated by strongly pinned DP, leaving the remaining part of the sample with weakly pinned OP, and resulting in a large voltage response. With increasing frequency the time of injection of the DP decreases and the width of the contaminated areas close to the edges shrinks.

To verify the EC model predictions we have measured the self-induced field  $B_{ac}(x)$  of the a.c. transport current using linear arrays of miniature Hall sensors and a lock-in detection technique [34, 35]. The Hall probes are based on the two-dimensional electron gas (2DEG) in AlGaAs/GaAs heterostructures grown on undoped semi-insulating GaAs substrates by means of molecular beam epitaxy [54]. The array comprises eleven  $10 \times 10 \mu\text{m}^2$  Hall sensors, connected in series with a  $30 \mu\text{m}$  separation between them. The 2DEG resides  $0.1 \mu\text{m}$  below the surface. Their sensitivity to fields normal to the 2DEG is of the order of  $100 \text{ m}\Omega/\text{gauss}$ . These structures provide significantly better spatial resolution than SQUID sensors and operate better in a changing temperature environment.  $B_{ac}(x)$  can be directly inverted into a current density distribution using the Biot-Savart law, as described elsewhere [34]. The resulting  $J_{ac}(x)$  distributions are shown in Fig. 4. When a significant d.c. current  $I_{dc} = 5.7 \text{ mA}$  is added to  $I_{ac} = 20 \text{ mA}$ , disordered vortices penetrate through the left edge of the sample and contaminate a significant part of the sample (Fig. 4a). Accordingly, as proven by the measured  $J_{ac}(x)$  distribution, the majority of the current flows along the left edge occupied by DP with high critical current. Upon reversal of the direction of the d.c. current (see Fig. 4b), DP is injected through the right edge of the sample and the distribution looks like a mirror image of that from Fig. 4a. However, when the d.c. component is very weak compared to the a.c. current amplitude, as in the case illustrated in Fig. 4c for  $I_{dc} = 1.7 \text{ mA}$ , the contamination by the DP is restricted to two relatively narrow bands at the sample edges.

The frequency dependence of  $J_{ac}(x)$  distributions is illustrated in Fig. 5. At high frequencies, the DP with enhanced  $J_c$  is present only in the narrow regions close to the edges (481 Hz data). At 181 Hz the DP areas grow and, correspondingly, the enhanced  $J_{ac}(x)$  flows in wider regions near the edges. When the frequency is reduced to 22 Hz the disordered border regions overlap and the enhanced current flows through entire sample width. The actual measured  $J_{ac}(x)$  is the magnitude of the local current density averaged over the cycle period. Close to the edges, the high  $J$  is present most of the time,

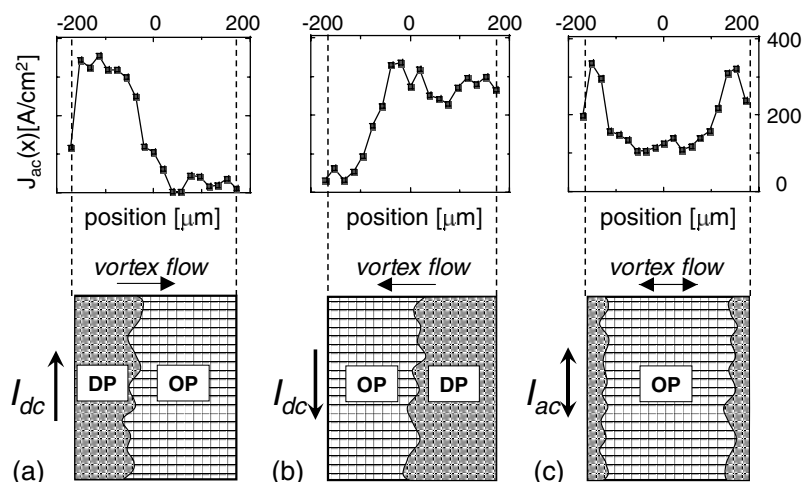


**Fig. 4.** a.c. current density distributions. (a)  $I_{dc} = 5.7$  mA; DP is injected through the left edge, DP occupies a substantial part of the sample. (b) Reversed direction of current flow  $I_{dc} = -5.7$  mA. (c)  $I_{dc} = 1.7$  mA; at small d.c. bias  $I_{dc} \ll I_{ac}$  the current distribution is similar to the zero d.c. bias case and peaks at the sample edges. The applied a.c. current has the same amplitude of 20 mA and frequency of 181 Hz in all cases

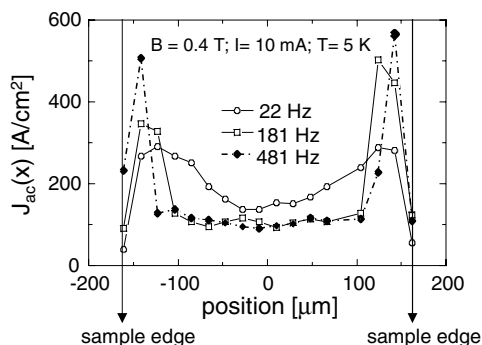


**Fig. 5.** Current density profiles  $J_{ac}(x)$  obtained by inversion of the self-induced field measured by Hall sensors at frequencies  $f = 22$  Hz (circles), 181 Hz (open squares), and 481 Hz (solid squares). The width of the disordered phase near the edges grows with decreasing frequency

while at the depth corresponding to the a.c. penetration depth of the DP, high current density persists only during a small fraction of the a.c. period since the DP continuously moves in and out of the sample. Therefore, the measured amplitude of the time-averaged  $J_{ac}(x)$  decreases smoothly from the sample edge to the point determined by the a.c. penetration depth, (see Fig. 5).

The behavior of the a.c. response illustrated in Fig. 3 is a natural consequence of the EC mechanism. As follows from the profiles in Fig. 4, the addition of a small d.c. component to the a.c. current contaminates the sample very similarly to the pure d.c. case, except that the penetration depth of the DP is reduced. When  $I_{dc} \ll I_{ac}$  the vortices move back and forth during the a.c. cycle, with a forward displacement being enhanced by about  $2I_{dc}/I_{ac}$ . Because the annealing process of the disordered vortex phase depends on the total displacement, regardless of the direction, the DP is thus annealed more efficiently. Therefore, at very small d.c. currents, the disordered phase is present only close to the edges where the DP exits and re-penetrates during every half-cycle. Vortices that drift deeper into the bulk are practically fully annealed. As a result, the initial decrease of  $R_{ac}$  for currents below 2mA in Fig. 4 is relatively small. With increasing d.c. current DP penetrates deeper into the sample leading to a marked drop in the a.c. response. The above mechanism accounts for the finite a.c. response and explains why the addition of a relatively small d.c. bias or asymmetry in the  $I_{ac}$  waveform dramatically suppresses the vortex motion.

The EC mechanism, by causing frequency, amplitude and direction-dependent distributions of current density, accounts also for the memory effects. The history of the previously applied current is encoded in the spatial profile of the lattice disorder, which in low temperature superconductors, such as NbSe<sub>2</sub>, is preserved after the current is switched off owing to negligible thermal relaxation. On reapplying the current, the vortex system will display a memory of all the parameters of the previously applied current, including its direction, duration, amplitude and frequency.

## 4 Low Frequency Noise

The appearance of large, broadband, low frequency noise with the onset of motion of a condensate in the presence of a quenched random pinning potential (jamming), has been studied extensively in incommensurate charge density waves [36], Wigner crystals in two-dimensional electron gas [37], and most notably, in vortex matter in type-II superconductors [19,20,29–32,38–49,51–53]. In all cases, the noise is thought to represent spatio-temporal irregularities of the moving condensate due to its interaction with the underlying pinning potential, but its precise origin remains obscure and controversial. The voltage noise due to vortex motion in a current-biased superconductor is generally referred to as flux-flow noise for which various specific mechanisms have been considered (for a review of early results see [38]). They include vortex shot noise and the associated density fluctuations [30,32,38–41], velocity fluctuations resulting from vortex-pin interactions [38], or turbulent flow of surface currents [42], critical slowing down of vortex dynamics [44], and several suggestions [19,20,29,45–47] and numerical simulations [48,49,51] of various plastic vortex flow mechanisms. Each of

these mechanisms may make a substantial contribution to the total measured noise. Yet the puzzling observation, which has no satisfactory explanation, is that in a specific and narrow region of the  $H - T$  phase diagram the noise is enhanced drastically. This unconventional noise, which we refer to as excess noise, exceeds the usual flux-flow noise level by orders of magnitude [19, 20, 29, 38, 45, 46]. In low- $T_c$  superconductors the excess noise occurs in the vicinity of the peak effect (PE) below  $H_{c2}$ , where the critical current  $I_c$  anomalously increases with field [19, 20, 38, 45]. In high- $T_c$  superconductors similar noise enhancement was found in the vicinity of the melting or order-disorder transitions [27–29, 46]. This low frequency excess noise is apparently inconsistent with the common flux-flow noise mechanisms due to its unusually high amplitude, strong field and current dependence, and frequently observed non-Gaussian character [19, 20, 29, 45].

#### 4.1 Simplified Model of the Noise

The generation of the metastable DP is a random process due to the non-uniform penetration of vortices through the surface barrier. As a result, the degree of vortex-lattice disorder and the corresponding value of  $J_c^{dis}$  at the sample edge are random functions of time. Similarly, annealing of the flowing DP is a random process that can be taken into account by considering  $L_r$  to be a random variable. Since  $J_c^{dis}$  is typically an order of magnitude larger than  $J_c^{ord}$  [6], random variations  $\delta J_c^{dis}$  and  $\delta L_r$  will result in large fluctuations of the integrated critical current of the sample, causing large voltage noise.

The  $V(I)$  curve in the vicinity of the peak effect is described by  $V(I) = R_f[I - I_c(V)]$ , where  $I_c$  is given by 2. In the small signal approximation we separate voltage fluctuations into two terms:

$$\delta V(I) \approx \frac{\partial V(I)}{\partial I_c} \delta I_c + \frac{\partial V(I)}{\partial R_f} \delta R_f . \quad (3)$$

By defining the differential resistance as

$$R_d \equiv \frac{\partial V}{\partial I} = -\frac{\partial V}{\partial I_c} , \quad (4)$$

(3) becomes

$$\delta V(I) = -R_d \delta I_c + \frac{V(I)}{R_f} \delta R_f . \quad (5)$$

Since experimentally  $L_r$  is usually smaller than  $W$  we can approximate (2) by  $I_c \simeq L_r d(J_c^{dis} - J_c^{ord}) + W dJ_c^{ord}$  [5]. In this approximation the fluctuation of the total critical current is

$$\delta I_c \approx d\delta \tilde{J}_c(0) L_r + d\tilde{J}_c(0) \delta L_r . \quad (6)$$

From Eg. 5 we obtain that

$$\delta V(I) \approx -dR_d \tilde{J}_c(0) L_r \left[ \frac{\delta \tilde{J}_c}{\tilde{J}_c} + \frac{\delta L_r}{L_r} \right] + V(I) \frac{\delta R_f}{R_f}. \quad (7)$$

We now write the power spectral density (PSD) of the voltage noise as

$$S_V \approx d^2 R_d^2 \tilde{J}_c^2(0) L_r^2 S_{in/ann} + V^2 S_{r_f}, \quad (8)$$

where  $S_{r_f} = S_{R_f}/R_f^2$  is the normalized spectral density of the flux-flow resistance fluctuations and  $S_{in/ann}$  is the normalized spectral density of the vortex injection and annealing noise. The most important conclusion that will enable us to understand the dependence of excess noise on applied magnetic field and current is that the noise intensity is proportional to  $R_d^2 \tilde{J}_c^2(0) L_r^2$ .

## 4.2 Experimental Results

The most direct test of the EC noise mechanism is the comparison of the Corbino disk noise with that of the strip, as shown in Fig. 6. In the Corbino the excess noise is almost entirely absent, indicating that the randomness in motion of the vortex lattice within the bulk of the sample does not, by itself, create excess noise. The absence of the noise in the Corbino clearly indicates the dominant role of edge contamination in the noise process. The residual small and narrow peaks in the Corbino noise in Fig. 6 can be ascribed to small deviations from a perfect Corbino disk configuration. Since  $L_r$  diverges at  $H_{DT}$ , any small non-radial part of the current may result in some injection of the metastable DP, giving rise to noise. Similarly, small inhomogeneities in the quenched disorder may result in a slightly position-dependent  $H_{DT}$ . In this case, in a narrow field region in the vicinity of the mean-field  $H_{DT}$  some parts of the sample are in the equilibrium DP, whereas others are in the OP. When the entire lattice is set in motion the DP drifts into regions of the OP, where it becomes metastable, and may cause noise in this narrow field region.

In contrast, the strip noise is very pronounced. The peak of the noise around 3.5 kOe in Fig. 6 is a result of the large  $L_r$  in the vicinity of the phase transition. The second noise peak at about 2 kOe marks the reentrant phase transition at which  $L_r$  becomes large again on approaching  $H_{DT}$ . This low-field peak was not previously observed since the noise studies were carried out on undoped NbSe<sub>2</sub> [19,20,45] which does not show a pronounced reentrant disorder-driven transition. The existence of two peaks demonstrates that the excess noise is not a mere result of the fact that  $I_c$  increases with  $H$  at the PE since at low fields the same excess noise is found in the region where  $I_c$  decreases with  $H$ . Furthermore, the same value of  $I_c$  is attained at three values of  $H$ : above the reentrant  $H_{DT}$  where  $I_c$  decreases with  $H$ , below the high field  $H_{DT}$  where  $I_c$  increases with  $H$ , and in the upper part of the PE, above the high field  $H_{DT}$  where  $I_c$  decreases again with  $H$ . The excess noise occurs only in the first two cases, where the metastable DP

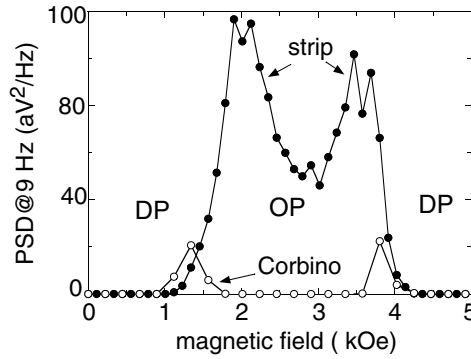


**Fig. 6.** Power spectral density of noise at 9 Hz and  $T = 4.4$  K in Corbino (*open circles*) and strip (*solid circles*) geometries. The currents in the Corbino and strip geometries were adjusted to provide equal current densities in the vicinity of the voltage contacts for both geometries

contaminates the equilibrium OP. In the third case, above  $H_{DT}$ , the DP is the thermodynamically stable phase and therefore no “wrong” phase is generated at the edges.

Figure 7 shows the intensity of the strip noise  $S_V^{1/2}$ , seen at a selected frequency of 3 Hz, as a function of bias current, along with the  $V - I$  characteristics for two different values of applied magnetic field. In each case, the onset of the noise coincides with the onset of d.c. current induced dissipation. With increasing current the  $I - V$  curve shows an upturn and eventually approaches linear flux-flow behavior at elevated currents. The noise displays a large peak and then vanishes rapidly at higher currents. Assuming for simplicity that

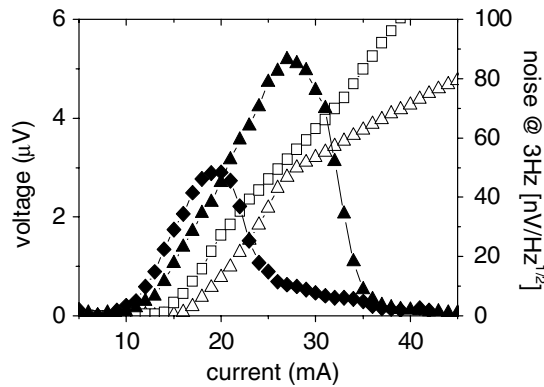


**Fig. 7.**  $V - I$  characteristics (*open symbols*) and spectral intensity of the noise (*solid symbols*) at 3 Hz as a function of bias current at 4.2 K: triangles – 2 kOe, diamonds – 3 kOe

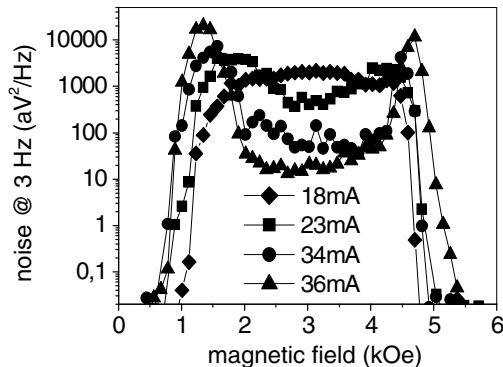


**Fig. 8.** Power spectral density of the strip noise at a fixed frequency of 3 Hz as a function of magnetic field at various bias currents.  $T = 4.2$  K

$\delta J_c^{dis}$  is current independent, the dominant parameters affecting the noise intensity are the relaxation length  $L_r$  and the differential resistance  $R_d$  (see (8)).

The initial buildup of the noise with increasing current follows the initial growth of  $R_d$ . The subsequent decay of the noise is the result of a decrease of  $L_r$  with increasing vortex velocity. Indeed, above 28 mA the  $V - I$  characteristic approaches the linear behavior of the OP, indicating that most of the sample volume is in the OP and that  $L_r$  is small. Since the ordered part of the sample does not contribute to the noise, the noise vanishes as the width of the DP near the edge shrinks to zero. The specific details of the above qualitative description are expected, however, to be significantly more complicated because of several factors, including the possible current dependence of  $\delta J_c^{dis}$  and the fact that  $\delta V$  is often comparable to  $V$ , resulting in a highly nonlinear and apparently non-Gaussian response [19,20], for which the above oversimplified analysis is not valid.

The above considerations facilitate the analysis of the general behavior of the strip noise shown in Fig. 8. At low currents ( $<18$  mA), vortex motion occurs only in the central field region far away from  $H_{DT}$ . In the vicinity of the transition the integrated  $I_c$  of the strip is larger than the driving current due to the large  $L_r$ . As a result, the excess noise is present only in the central field range. At 23 mA, the range of fields, for which vortex motion and the corresponding noise are observable, expands and two noise peaks become readily apparent. In the central region the DP is less stable,  $L_r$  drops with  $I$ , and hence the noise decreases rapidly with current. Closer to the transition fields, however, the metastable DP is much more stable and therefore even at 23 mA  $L_r$  remains large and noise is still increasing with current. At 36 mA most of the sample is already in the OP and the noise in the central field range has accordingly dropped by two orders of magnitude. The strong excess

noise is restricted now only to the narrow regions adjacent to the transition fields where the metastable DP survives even at high vortex velocities.

### 4.3 Velocity vs. Density Fluctuations

The electric field due to magnetic flux motion with a velocity  $v$ , neglecting voltages induced by variations of the flux threading the loop enclosed by the voltage leads, can be written simply as  $\mathbf{E} = -\mathbf{v} \times \mathbf{B}$ . The voltage fluctuations  $\delta V(t) = V(t) - \bar{V}$ , where  $\bar{V} = vBl$  is the d.c. voltage, can be due either to the fluctuations of magnetic field  $\delta \mathbf{B} = \Phi_0 \delta n \mathbf{B} / B$ , where  $\delta n$  are the fluctuations in the vortex density  $n$ , or to the fluctuations of the vortex velocity  $\mathbf{v}$ . In a small signal approximation

$$\delta V \approx l(v\delta B + B\delta v). \quad (9)$$

The first term contains density fluctuations  $\delta n = n(t) - \bar{n}$ , where  $\bar{n} = B/\Phi_0 = N/Wl$  is the equilibrium vortex density and  $N$  is the total number of vortices. Vortex density fluctuations can be therefore directly evaluated by measuring the associated magnetic field noise. The second term describes velocity fluctuations  $\delta v = v(t) - \bar{v}$ , where the equilibrium vortex velocity  $\bar{v} = \bar{V}/Bl$ . Alternatively, the fluctuating component of the voltage due to current driven vortex motion is given by (3). Direct comparison of (9) with (5) suggests to associate vortex density fluctuations with the fluctuations of the flux-flow resistance  $\delta R_f$  and fluctuations of the vortex velocity with the fluctuations of the critical current  $\delta I_c \propto \delta \tilde{J}_c(0)$ .

In the experiments we have measured simultaneously the voltage and magnetic field noise associated with the current driven vortex motion. After sufficiently long thermalization at low temperatures the Hall sensor d.c. bias current level that causes onset of the excess shot noise was well above 200  $\mu\text{A}$  enabling us to operate safely at high current bias, what significantly improves the signal to noise ratio of the sensor. The ultimate sensitivity of our flux detection system was typically better than  $2 \times 10^{-7}$  T/Hz<sup>1/2</sup> at frequencies above 5 Hz.

To perform simultaneous conduction and magnetic noise measurements the NbSe<sub>2</sub> crystal with attached leads was placed directly on top of the Hall sensor array. The entire arrangement was immersed in a specially designed low noise variable temperature cryostat equipped with an external  $\mu$ -metal shield and a superconducting magnet operating in persistent mode. In each experimental run the sample was zero-field cooled to the required temperature before application of the magnetic field and bias current. The sample voltage, measured in a four-point contact arrangement, and the Hall probe signal were brought to the top of the cryostat by twisted-pairs, amplified by home-made low noise voltage preamplifiers located within the cryostat head, and processed by a computer-assisted spectrum analyzer. The power spectra of the flux and voltage fluctuations were recorded simultaneously with the

time domain records and d.c. voltage response. Instrumental noise originating in the measurement circuit, was recorded at zero current through the NbSe<sub>2</sub> crystal and subsequently subtracted from the spectra measured in the presence of bias.

We have searched for flux noise manifestations in the entire range of currents, magnetic fields, and temperatures at which the excess voltage noise appears. Within the sensitivity of our Hall probe arrangement we could not detect any vortex density fluctuations. Even by biasing the sample at the very noise peak, where the voltage noise spectral intensity increases more than four orders of magnitude above the preamplifier background, we saw no difference in the magnetic noise detected with and without the application of the driving current causing the motion and annealing of the vortex lattice.

In the face of the negative result we carefully checked that the Hall probe was properly coupled to the sample by measuring the Meissner effect at low fields and the self-induced a.c. field of an a.c. transport current. All tests proved unambiguously that the Hall sensors were properly coupled.

The absence of density fluctuations, in fact, is not surprising and is consistent with the EC model predictions. Let us rewrite the total spectral density of the voltage noise (5) in terms of the normalized spectral density  $S_v = S_V/V^2$ :

$$S_v = \frac{1}{R_f^2} S_{R_f} + \frac{R_d^2}{V^2} S_{I_c} . \quad (10)$$

By plotting the normalized voltage noise spectral density as a function of the ratio  $R_d^2/V^2$  one can separate contributions of the fluctuating vortex density and velocity to the total noise. The PSD value for  $R_d^2/V^2 = 0$  corresponds to  $S_{R_f}$ , which in turn describes vortex density fluctuations, while the slope of the  $S_v(R_d^2/V^2)$  plot gives the spectral density of the critical current fluctuations  $S_{I_c}$ .

The experimental data at 0.2 T from Fig. 1 are plotted in the above coordinate system in Fig. 9. The data fit very well to a straight line passing through the origin. It clearly demonstrates that the excess noise due to the contamination mechanism is entirely dominated by the critical current fluctuations causing large voltage noise by inducing strong fluctuations of the velocity of moving vortices. According to (10) any significant density fluctuations would offset the linear fit upward, such that it would cross the y-axis at the value corresponding to  $S_R$ . This is clearly not the case in Fig. 2.

We conclude that the excess flux-flow noise in the vicinity of the peak effect is entirely dominated by vortex velocity fluctuations resulting from the critical current fluctuations due to random injection and random annealing of the metastable disordered vortex phase. This result may seem surprising in view of the experimental evidence of local vortex density noise associated with current driven motion of vortices in high- $T_c$  Bi<sub>2</sub>Sr<sub>2</sub>CaCu<sub>2</sub>O<sub>y</sub> (BSCCO) single crystals [30–32]. The flux noise in BSCCO system has been detected using a Hall probe with similar sensitivity. The major difference between

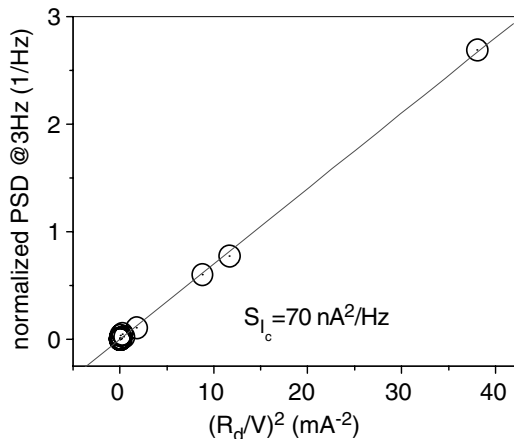


**Fig. 9.** Data points at 2 kOe from Fig. 7 plotted as a normalized power spectral density as a function of  $R_d^2/V^2$ . Observe that the best linear fit to the data passes through the origin indicating that the voltage noise is due entirely to the critical current fluctuations (see text)

the two systems is the fact that in the low- $T_c$  Nb<sub>2</sub>Se the excess noise is associated with order-disorder transitions within the solid state of the vortex matter, whereas in high- $T_c$  BSCCO the excess noise can be associated with the melting transition. Since the vortex liquid has higher density than the solid, local melting transitions may result in strong density fluctuations. Nevertheless, it has been shown that the order-disorder phase transition in the solid vortex phase is also associated with a magnetization jump which should result in similar density fluctuations [55, 56]. A possible reason for the lack of measurable density fluctuations at the solid-solid phase transition is the very slow dynamics with which the equilibrium magnetization is reached. In fact, to detect the magnetization step at the disorder-driven phase transition the special experimental technique of vortex dithering had to be applied [55]. For this reason density fluctuations, if any, may appear at very low frequencies, much lower than the frequencies at which the excess voltage noise has been observed and beyond the spectral range of the experiment. The exact reason for the different aspects of excess noise in low and high- $T_c$  systems remains, however, an open question.

## 5 Conclusions

In summary, we have shown that the ordered Bragg glass phase becomes unstable with respect to disorder at both high and low fields, resulting in a reentrant disorder-driven transition. By using a Corbino geometry, and thus

avoiding the contamination from the sample edges, we have shown that this transition is very sharp and apparently of first order.

The injection of the disordered phase through the sample edges causes a nonuniform distribution of the pinning strength and, correspondingly, a nonuniform distribution of the current density. In the restricted areas of the phase diagram, in the vicinity of the peak effect, the disordered phase dynamically coexists with the ordered phase, giving rise to a plethora of exotic phenomena in the vortex matter dynamics. It follows from the proposed edge contamination model that the transport current has two antagonistic effects; injection of the disordered phase at the sample edge and its annealing in the bulk. The edge contamination model explains the memory effects in vortex matter by the history of the previously applied current being encoded in the spatial profile of the lattice disorder, which cannot be erased by negligible thermal fluctuations at low temperatures.

The excess flux-flow noise appearing in the vicinity of the peak effect has been associated with edge contamination and has been shown not to result from mere random motion of vortices in the bulk of the sample. The main conceptual difference is that in the conventional models only random vortex penetration or irregular vortex motion in the bulk is considered. We have considered randomness in the injection and annealing processes of the metastable disordered phase resulting in large fluctuations in the instantaneous critical current of the sample, leading to very large voltage noise. We have demonstrated that the excess noise can be eliminated by preventing the edge contamination in the Corbino disk geometry. Direct flux noise measurements and re-examination of the voltage noise data brought us to conclusion that the excess flux-flow noise is entirely dominated by vortex velocity fluctuations resulting from the critical current fluctuations. We believe that the new noise mechanism may be of importance for various condensed matter systems exhibiting similar noise associated with a fluctuating pinning force such as incommensurate charge density waves or Wigner crystals in two-dimensional electron gas.

## Acknowledgments

This work was supported by the Israel Science Foundation - Center of Excellence Program, by the United States-Israel Binational Science Foundation (BSF), and by the German-Israeli Foundation for Scientific Research and Development (GIF).

## References

1. G. Blatter, M. V. Feigelman, V. B. Geshkenbein, A. I. Larkin, V. M. Vinokur: *Rev. Mod. Phys.* **66**, 1125 (1994).

2. G. W. Crabtree and D. R. Nelson: *Phys. Today* **50**, 38 (1997).
3. S. Kuriki, S. Hirano, A. Maeda, T. Kiss: *Topics in Appl. Phys.* **91**, 5 (2003).
4. G. W. Crabtree: *Nature Mat.* **2**, 435 (2003).
5. Y. Paltiel, E. Zeldov, Y. N. Myasoedov, H. Shtrikman, S. Bhattacharya, M. J. Higgins, Z. L. Xiaok, E. Y. Andrei, P. L. Gammel and D. J. Bishop: *Nature* **403**, 398 (2000).
6. Y. Paltiel, E. Zeldov, Y. Myasoedov, M. L. Rappaport, G. Jung, S. Bhattacharya, M. J. Higgins, Z. L. Xiao, E. Y. Andrei, P. L. Gammel, and D. J. Bishop: *Phys. Rev. Lett.* **85**, 3712 (2000).
7. M. Marchevsky, M. J. Higgins, and S. Bhattacharya: *Phys. Rev. Lett.* **88**, 087002 (2002).
8. S. Bhattacharya and M. J. Higgins: *Phys. Rev. B* **52**, 64 (1995).
9. W. Henderson, E. Y. Andrei, M. J. Higgins, and S. Bhattacharya: *Phys. Rev. Lett.* **77**, 2077 (1996).
10. Song Yue, Bo Zhang, Shun Tan, Mingliang Tian and Yuheng Zhang: *Europhys. Lett.* **66**, 272 (2004).
11. M. Menghini, Y. Fasano and F. de la Cruz: *Phys. Rev. B* **65**, 064510 (2002).
12. P. Benetatos and M. C. Marchetti: *Phys. Rev. B* **65**, 134517 (2002).
13. S. Okuma and M. Kamada: *Phys. Rev. B* **70**, 014509 (2004).
14. Y. Paltiel, E. Zeldov, G. Jung, Y. Myasoedov, M. L. Rappaport, D. Feldman, M. J. Higgins, and S. Bhattacharya: *Phys. Rev. B* **66**, 060503R (2002).
15. M. Gitterman: *Phys. Rev. E* **70**, 036116 (2004).
16. B. Y. Shapiro, M. Gitterman, I. Shapiro: *Physica C* **388**, 681 (2003).
17. K. Ghosh, S. Ramakrishnan, A. K. Grover, Gautam I. Menon, Girish Chandra, T. V. Chandrasekhar Rao, G. Ravikumar, P. K. Mishra, V. C. Sahni, C. V. Tomy, G. Balakrishnan, D. Mck Paul, S. Bhattacharya: *Phys. Rev. Lett.* **76**, 4600 (1996).
18. S. S. Banerjee, N. G. Patil, S. Ramakrishnan, A. K. Grover, S. Bhattacharya, P. K. Mishra, G. Ravikumar, T. V. Chandrasekhar Rao, V. C. Sahni, M. J. Higgins, C. V. Tomy, G. Balakrishnan, and D. Mck. Paul: *Europhys. Lett.* **44**, 91 (1998).
19. A. C. Marley, M. J. Higgins, and S. Bhattacharya: *Phys. Rev. Lett.* **74**, 3029 (1995).
20. R. D. Merithew, M. W. Rabin, M. B. Weissman, M. J. Higgins and S. Bhattacharya: *Phys. Rev. Lett.* **77**, 3197 (1996).
21. S. S. Banerjee, N. G. Patil, S. Saha, S. Ramakrishnan, A. K. Grover, S. Bhattacharya, G. Ravikumar, P. K. Mishra, T. V. Chandrasekhar Rao, V. C. Sahni, M. J. Higgins, E. Yamamoto, Y. Haga, M. Hedo, Y. Inada, Y. Onuki: *Phys. Rev. B* **58**, 995 (1999).
22. S. S. Banerjee, N. G. Patil, S. Ramakrishnan, A. K. Grover, S. Bhattacharya, G. Ravikumar, P. K. Mishra, T. V. Chandrasekhar Rao, and V. C. Sahni, M. J. Higgins: *Appl. Phys. Lett.* **74**, 126 (1999).
23. Y. Liu, H. Luo, X. Leng, Z. H. Wang, L. Qiu, S. Y. Ding, and L. Z. Lin: *Phys. Rev. B* **66**, 144510 (2002).
24. W. Henderson, E. Y. Andrei and M. J. Higgins: *Phys. Rev. Lett.* **81**, 2352 (1998).
25. Z. L. Xiao, E. Y. Andrei and M. J. Higgins: *Phys. Rev. Lett.* **83**, 1664 (1999).
26. R. Schleser, P. J. E. M. van der Linden, P. Wyder, A. Gerber: *Phys. Rev. B* **67**, 134516 (2003).

27. S. N. Gordeev, P. A. J. deGroot, M. Oussena, A. V. Volkozub, S. Pinfeld, R. Langan, R. Gagnon, L. Taillefer: *Nature* **385**, 324 (1997).
28. W. K. Kwok, G. W. Crabtree, J. A. Fendrich, L. M. Paulius: *Physica C* **293**, 111 (1997).
29. G. D'Anna, P. L. Gammel, H. Safar, G. B. Alers, D. J. Bishop, J. Giapintzakis, D. M. Ginsberg: *Phys. Rev. Lett.* **75**, 3521 (1995).
30. T. Tsuboi, T. Hanaguri, and A. Maeda: *Phys. Rev. Lett.* **80**, 4550 (1998).
31. Y. Togawa, R. Abiru, K. Iwaya, H. Kitano, and A. Maeda: *Phys. Rev. Lett.* **85**, 3716 (2000).
32. A. Maeda, T. Tsuboi, R. Abiru, Y. Togawa, H. Kitano, K. Iwaya, T. Hanaguri: *Phys. Rev. B* **65**, 054506 (2002).
33. S. Kokkaliaris, P. A. J. de Groot, S. N. Gordeev, A. A. Zhukov, R. Gagnon and L. Taillefer: *Phys. Rev. Lett.* **82**, 5116 (1999).
34. Y. Paltiel, D. T. Fuchs, E. Zeldov, Y. N. Myasoedov, H. Shtrikman, M. L. Rappaport, E. Y. Andrei: *Phys. Rev. B* **58**, R14763 (1998).
35. D. T. Fuchs, E. Zeldov, M. Rappaport, T. Tamegai, S. Ooi, H. Shtrikman: *Nature* **391**, 373 (1998).
36. S. Bhattacharya, J. P. Stokes, Mark O. Robbins, and R. A. Klemm: *Phys. Rev. Lett.* **54**, 2453 (1985).
37. Yuan P. Li, T. Sajoto, L. W. Engel, D. C. Tsui, and M. Shayegan: *Phys. Rev. Lett.* **67**, 1630 (1991).
38. J. R. Clem: *Phys. Rep.* **75**, 1 (1981).
39. W. J. Yeh and Y. H. Kao: *Phys. Rev. B* **44**, 360 (1991).
40. V. D. Ashkenazy, G. Jung, and B. Ya. Shapiro: *Physica C* **254**, 77 (1995).
41. K. E. Gray: *Phys. Rev. B* **57**, 5524 (1998).
42. B. Placais, P. Mathieu, and Y. Simon: *Phys. Rev. Lett.* **70**, 1521 (1993)
43. B. Placais, P. Mathieu, and Y. Simon: *Phys. Rev. B* **49**, 15813 (1994).
44. P. J. M. Wöltgens, C. Dekker, S. W. A. Gielkens, and H. W. de Wijn: *Physica C* **247**, 67 (1995).
45. M. W. Rabin, R. D. Merithew, M. B. Weissman, M. J. Higgins and S. Bhattacharya: *Phys. Rev. B* **57**, R720 (1998).
46. H. Safar, P. L. Gammel, D. A. Huse, G. B. Alers, D. J. Bishop, W. C. Lee, J. Giapintzakis, and D. M. Ginsberg: *Phys. Rev. B* **52**, 6211 (1995).
47. S. Okuma and N. Kokubo: *Phys. Rev. B* **61**, 671 (2000).
48. I. Aranson and V. Vinokur: *Phys. Rev. Lett.* **77**, 3208 (1996).
49. C. J. Olson, C. Reichhardt, and F. Nori: *Phys. Rev. Lett.* **80**, 2197 (1998).
50. A. B. Kolton, D. Dominguez, and N. Gronbech-Jensen et al: *Phys. Rev. Lett.* **83**, 3061 (1999).
51. M. C. Marchetti, A. A. Middleton, and T. Prellberg: *Phys. Rev. Lett.* **85**, 1104 (2000).
52. Y. Paltiel, G. Jung, Y. Myasoedov, M. L. Rappaport, E. Zeldov, S. Bhattacharya, M. J. Higgins: *Europhys. Lett.* **58**, 112 (2002).
53. Y. Paltiel et al: *Europhys. Lett.* **66**, 412 (2004)
54. E. Zeldov, D. Majer, M. Konczykowski, V. B. Geshkenbein, V. M. Vinokur, H. Shtrikman: *Nature* **375**, 373 1995.
55. N. Avraham, B. Khaykovich, Y. Myasoedov, M. Rappaport, H. Shtrikman, D. E. Feldman, T. Tamegai, P. H. Kes, M. Li, M. Konczykowski, K. van der Beek, E. Zeldov: *Nature* **411**, 451 2001.
56. G. Ravikumar, P. K. Mishra, V. C. Sahni, S. S. Banerjee, S. Ramakrishnan, A. K. Grover, P. L. Gammel, D. J. Bishop, E. Bucher, M. J. Higgins and S. Bhattacharya: *Physica C* **332**, 145 (1999).